Lattice dynamics of rare-earth semiconductors with unstable valence

1991 J. Phys.: Condens. Matter 3 5937

(http://iopscience.iop.org/0953-8984/3/32/003)

J. Phys.: Condens. Matter 3 (1991) 5937–5954. Printed in the UK

Lattice dynamics of rare-earth semiconductors with unstable valence

A S Mishchenko and K A Kikoin
I V Kurchatov Institute of Atomic Energy, 123182 Moscow, USSR

Received 5 March 1991

Abstract. The phonon spectra of rare-earth (RE) semiconductors with integer and mixed valence (EuS, SmS, TmSe) are calculated within the generalized charge-density distortion model. The model includes interaction of lattice vibrations with the valence shell excitations, both local (usual dipole excitations in unfilled shells of RE ions) and non-local breathing modes describing the valence fluctuations. The relative contribution of these excitations to phonon renormalization is traced along the row of RE semiconductors with rock-salt structure.

1. Introduction

The lattice dynamics of rare-earth (RE) semiconductors with unstable valence (Sm and Tm chalcogenides and Sm hexaboride) is described in general terms by the charge-density deformation (CDD) model proposed by Allen more than 10 years ago (Allen 1977). This theory explained in general the anomalies in the LA [1 1 1] branch of the phonon spectra of SmS and TmSe (Bilz *et al* 1979, Bennemann and Avignon 1979, Entel *et al* 1979, Matsuura *et al* 1980, Wakabayashi 1980, Ichinose and Kuroda 1982, Ichinose and Tamura 1983). Although these authors refer to the valence fluctuations as the source of the breathing charge mode, there is no real microscopic substantiation of the valence fluctuation contribution to the dynamic matrix because of many simplifications accompanying the calculation of the electron–phonon renormalization of the phonon spectra. Moreover, detailed analysis of the theoretical spectra shows some mismatches between the theory and experiment in both acoustic and optic branches.

In this paper we present a careful theoretical description of the phonon spectra of mixed-valence (MV) semiconductors with the rock-salt crystal structure in comparison with the 'reference' system EuS. When analysing the discrepancies between the theory, including breathing and dipole CDD modes, and the experimental data, we see the need to generalize the standard theory of local CDD modes and include the spatial dispersion of these modes, which in turn gives additional wavevector dispersion in the phonon renormalization, substantially improving the consistency between theory and experiment.

We propose microscopic grounds of non-local charge distortions specific for the mixed-valence systems. These are the anomalously soft fully symmetric excitonic modes, which are treated as the main source of valence fluctuations in the MV state of a semiconductor. The theory was checked recently by applying its results to an MV semi-

0953-8984/91/325937 + 18 $03.50

conductor with other than rock-salt symmetry, viz to SmB_6, for which phonon spectra were measured by the inelastic neutron spectroscopy method (Alexeev *et al* 1989).

We also analyse all other contributions to the phonon spectra of the RE semiconductors (long-range Coulomb forces, dielectric screening, impurity contamination, etc) and find that detailed analysis of dynamic properties strongly supports the microscopic picture of excitonic instability as a source of the phase transition from normal to MV semiconductor state of the RE compounds (Stevens 1976, Kikoin 1984).

2. Microscopic grounds of the CDD model for RE semiconductors

Our description of the lattice dynamics in RE semiconductors is based on the microscopic theory of the electron–phonon interaction in semiconductors with unstable valence, which was proposed in previous papers (Kikoin and Mishchenko 1988, 1990; hereafter referred to as KMI and KMII). The theory starts from the adiabatic procedure, which includes in the dynamic matrix the CDD contributions (Allen 1977)

$$D(q) = D^{\mathrm{RI}}(q) + D^{\mathrm{CDD}}(q) \tag{2.1}$$

where $D^{\mathrm{RI}}(q)$ is the Kellermann-type dynamic rigid-ion (RI) matrix for the purely ionic crystal, and the CDD component can be expanded as

$$D^{\mathrm{CDD}}(q) = \sum_{\Gamma} D^{\Gamma}(q). \tag{2.2}$$

This expansion reflects the possibility of classifying the CDD according to the irreducible representations of the crystal point group because of the local character of these electronic modes, which in turn can be expressed via the partial components of the charge-density response function χ_Γ

$$D^{\Gamma}(q) = N^{-1} \sum_{m,n} \mathrm{e}^{\mathrm{i}q(R_n - R_m)} \langle 0|\nabla_m H_{\mathrm{ei}}(r, R)\chi_\Gamma(r, r')\nabla_n H_{\mathrm{ei}}(r', R)|0\rangle \tag{2.3}$$

where

$$\chi_\Gamma(r, r') = |B^\Gamma\rangle\langle B^\Gamma|/(\omega - E^\Gamma_{\mathrm{ex}})$$

R_m are the lattice site indices, H_{ei} is the electron–ion interaction Hamiltonian, and $|B^\Gamma\rangle$ are the excited states of the electronic subsystem with point symmetry Γ and excitation energy E^Γ_{ex}. Various sources of the CDD modes were discussed in the literature (see e.g. Bilz and Kress 1979). We believe that in the RE semiconductors with unstable valence these are mainly exciton modes describing the charge distortions in unfilled f shells of lanthanide ions. It is well known from band structure calculations that the electrons from the 4f shell form a very narrow upper valence band, and the overlapping wavefunctions of 5d levels, which are empty in the ground state, form the lower part of the conduction band, at least in the RE chalcogenides with NaCl crystal structure. Hence there are several sources of local CDD induced by the f–d transitions. These are the interband transitions and intrashell Frenkel-type f–d excitations, which are commonly used to

explain the origin of monopole (breathing) and dipole CDD modes. These states can be presented as

$$|B^{\text{band}}_{q,k}) = N^{-1} \sum_{j,l} b^{+}_{j+l,c} b_{j,v} |0) \exp[-iq \cdot R_j - i(k+q) \cdot R_l] \tag{2.4}$$

$$|B^{\text{ex}}_{q\Gamma}) = N^{-1/2} \sum_{j} b^{+}_{j,c} b_{j,v} |0) \exp(iq \cdot R_j) \tag{2.5}$$

respectively. Here indices c, v stand for the conduction and valence band states, $|0)$ is the ground state of the semiconductor with filled valence band and empty conduction band, and index Γ of the point group irreducible representation is defined by the symmetry of the intrasite transition. Really $\Gamma = \Gamma^{-}_{15}$ for f–d transition in the deformable shell of Sm ions. In KMI and KMII we have proposed another source of monopole excitations. We think that the local charge distortions are naturally described in terms of intermediate-radius excitons

$$|B_{q\Gamma}) = N^{-1/2} \sum_{j,l} F(l) b^{+}_{j+l,c} b_{j,v} \exp(iq \cdot R_j). \tag{2.6}$$

Here $F(l)$ is the envelope function characterizing the spatial extension of the exciton. It was shown by Stevens (1976) and Kikoin (1984) (see also KMII) that the singlet exciton, i.e. the excited state of the same symmetry $^7F_0$ as the ground state of the Sm f shell, can be constructed by using an appropriate linear combination of conduction band d functions. This exciton can be treated as the source of relatively soft monopole (breathing) CDD with $\Gamma = \Gamma^{+}_{1}$ in integer-valence compounds like black $SmS_{(B)}$. The ground state of the mixed-valence compounds (gold $SmS_{(G)}$ and SmB_6) according to the theory of excitonic instability (Stevens 1976, Kikoin 1984) is considered as the bonding combination of ground and excited $^7F_0$ states of 'normal' semiconductor. Then the antibonding combination of these two states forms extremely soft monopole excitation specific for the mixed-valence semiconductor. This excitation greatly enhances the breathing CDD contribution to the dynamic matrix and can be treated as the main source of the anomalies in the phonon spectra.

Although the anomalously soft f–f electronic transitions were seen directly in the optical spectra of gold $SmS_{(G)}$ and SmB_6 (Travaglini and Wachter 1985), the idea of exciton–phonon renormalization of the phonon spectra should be carefully checked. We suppose that the non-local character of the excitonic contribution to the breathing CDD is a decisive moment that allows the verification of our proposals.

It was shown in KMII that in most cases the CDD contribution to the phonon frequency renormalization can be factorized as

$$\Delta_\Gamma \omega^2_{q,\alpha} = \lambda^{(\Gamma)}_{\alpha} \Phi^{(\Gamma)}(q, \omega_{q,\alpha}) \tag{2.7}$$

where the net q dependence of renormalization of the phonon branch α entering the form factor $\Phi^{(\Gamma)}$ depends only on the type of lattice and CDD symmetry, and the coupling strength $\lambda^{(\Gamma)}_{\alpha}$ is determined by the physical mechanisms 'switching on' this mode. It is clear that the spatial extension of the mode gives an additional contribution to the q dependence of form factor $\Phi^{(\Gamma)}(q)$, in comparison with the conventional local theory (Allen 1977), and this characteristic dependence allows one to detect the possible non-local contributions to the phonon renormalization.

Using the second-order approximate expression (2.7) for the phonon renormalization, we have shown in KMI and KMII that the quantitative consistency of the theory describing the CDD renormalization with the measured LA phonon dispersion in gold

$SmS_{(G)}$ can be improved essentially when accounting for the non-local character of CDD breathing mode. Here we use the more systematic approach including the non-local corrections directly to the dynamic matrix. In the case of two-sublattice crystal structure the CDD contribution (2.2) to this matrix can be represented in the form

$$D^{\Gamma_1^+}(q) = \begin{pmatrix} |G^{(1)}_{\Gamma_1^+}(q)|^2 |R_{\Gamma_1^+}(q)|^2 & 0 \\ 0 & |G^{(2)}_{\Gamma_1^+}(q)|^2 |R_{\Gamma_1^+}(q)|^2 \end{pmatrix} \tag{2.8}$$

where $G^{(1)}_{\Gamma_1^+}$ and $G^{(2)}_{\Gamma_1^+}$ are the standard CDD factors for the nearest-neighbour (NN) and next-nearest-neighbour (NNN) breathing interactions (Allen 1977) and $R_{\Gamma_1^+}$ is an additional 'covalent' factor due to the non-local character of the electron excitations B_q^Γ in (2.3) and (2.6). This covalent contribution in second-order perturbation theory results in additional q dependence of phonon renormalization, which takes the form

$$\Delta^{(\Gamma)}\omega^2_{q\alpha} = \lambda^\Gamma_\alpha \Phi^\Gamma_0(q, \omega_{q\alpha})\Phi^\Gamma_1(q, \omega_{q\alpha}) \tag{2.9}$$

where indices 0, 1 stand for the standard point CDD and non-local correction form factors, respectively.

When detecting the specific contribution of the soft CDD modes in RE semiconductors with unstable valence, we follow the procedure proposed in KMII, i.e. we study first the 'reference system' with stable valence in the framework of the standard CDD theory, and then compare the results of phonon calculation for the MV systems within the full non-local theory using dynamic matrix (2.1), (2.2) and (2.8) with the standard phonon branches of the normal RE semiconductor. Hence we can give a quantitative estimation of abnormal contribution to the electron–phonon renormalization, and speculate about the physical nature of that renormalization. We choose for the reference system the compound EuS, which is the closest neighbour of SmS in the row of RE chalcogenides having stable valence of 4f ion at ambient pressure.

3. Europium sulphide

Inelastic neutron scattering measurements of the phonon spectra are absent for EuS, and hence the phonon spectrum was restored from the macroscopic data, i.e. elastic moduli, dielectric susceptibility and ion polarizabilities, using only two phonon frequencies $\omega_{LO}(\Gamma)$ and $\omega_{TO}(\Gamma)$ (Zeyher and Kress 1979) in a framework of the overlap shell model (OSM) (see e.g. Bilz and Kress 1979, Bilz *et al* 1975). Zeyer and Kress used their spectra for calculating the Raman spectra and comparing them with the experiment of Güntherodt *et al* (1979). The excellent agreement between the theory and experiment allows us to consider these restored spectra as the basic ones for EuS. It should be noted, however, that the theoretical description within the OSM approach is inconsistent, because this model takes into account only the dipole CDD mode, whereas a more detailed symmetry analysis of the partial CDD contributions to the polarized Raman spectra shows the dominant contribution of the Γ_1^+ component of CDD on Eu ion to the first-order Raman spectrum in EuS.

Hence, we fit the 'basic' phonon spectrum of Zeyher and Kress (1979) by varying the parameters of our CDD model and include the breathing mode $G_{\Gamma_1^+} \equiv G_1$ to the dynamic matrix (2.8). Among the macroscopic force parameters the sulphur polarizability α_S is the most unreliable one. Zeyher and Kress used the value α_S obtained by Tessman *et al*

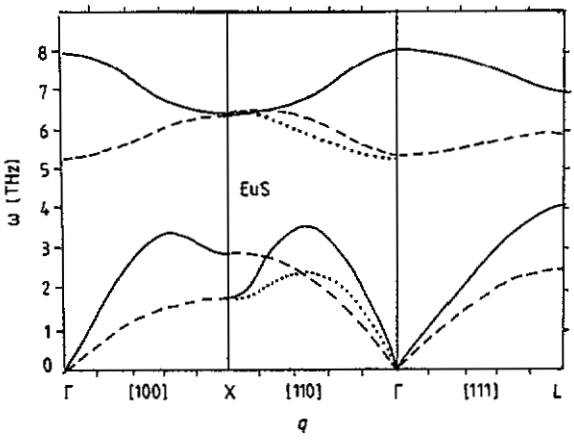

Figure 1. Calculated phonon spectrum of EuS in the modified model of Zeyher and Kress (1979). The sulphur polarizability $\alpha_2 = 4.40$ Å is taken lower than that in Tessman *et al* (1953). Monopolar CDD parameter $G_1 = 0.142\,e^2\,V^{-1}$. The theoretical curves are denoted as: (——) LA, LO; (– – –) TA_1, TO_1; (· · · · ·) TA_2, TO_2.

(1953) on the assumption of additivity of partial ion contributions to the total polarizability. This assumption is not so good for sulphides, and gives too high value of α, as can be seen from general expressions for the polarizability (Woods *et al* 1960). Hence, we varied α_S in a certain interval and defined the corresponding values of G_1 by fitting the LO(L) frequency of EuS, which is known from the polarized Raman scattering spectra. When lowering α_S from Tessman's value of 4.70 Å down to the value of 1.70 Å, we obtained values of G_1 from 0 up to $6.53\,e^2\,V^{-1}$. We have seen that varying α_S practically did not influence the form of the phonon spectra. Figure 1 shows the typical EuS spectrum.

Our analysis shows that, although the fully symmetric Γ_1^+ CDD mode should be introduced for the sake of complex description of the experimental data on the vibration spectrum, its value is small, and the real CDD contribution cannot be defined trustfully from fitting the theoretical curves to the experimental data available.

4. Samarium sulphide, black phase

We fitted our theoretical curves to the experimental neutron scattering spectra of Birgenau and Shapiro (1977). The LO branch of 'black' samarium sulphide ($SmS_{(B)}$) was not measured in that experiment, so we used the values $\omega_{LO}(\Gamma) = 7.26$ THz obtained from the optical measurements of dielectric response (Hillebrands and Güntherodt 1984) and $\omega_{LO}(L) = 6.0$ THz found in a Raman scattering experiment (Güntherodt *et al* 1981b). Symmetry degeneration of LO[1 0 0] and TO_1[1 1 0] frequencies at the X point gives us the third point in the LO branch.

The fitting procedure can be treated as the search for the global minimum of RMS deviation among many local ones in a multidimensional space of model parameters. We have tried several different fitting procedures and found that the best description of both macroscopic and microscopic data can be obtained within a framework of the model using measured dispersion curves together with the macroscopic elastic moduli and dielectric characteristics of the lattice. Various modifications of this 'hybrid model' are described in the appendix.

General softening of the electron excitation spectrum in $SmS_{(B)}$ in comparison with EuS implies the growing contribution of the CDD modes to the phonon renormalization (KMI, KMII). The usual description of the phonon spectra in SmS includes dipole CDD for both sublattices and breathing CDD for Sm ions (see e.g. Bilz *et al* 1979, Güntherodt *et al* 1981a). Calculated phonon spectra can be well fitted to the experimental points in [110] and [111] directions; however, the unusual softening of TO[100] branch near the X point discovered by Birgenau and Shapiro (1977) was not reproduced in those fittings. Using the general list of form factors (tables 1 and 2 in KMII) we find that the only source of such CDD renormalization (in NN approximation) is the tetragonal deformation mode Γ_{25}^-. Taking into account the symmetry of initial and final states for the local excitation from the top of the f valence band (Γ_{15}^-) to the $d(t_{2g})$ conduction band (Γ_{25}^+) (see e.g. Lopez-Aguilar and Costa-Quintana 1986), we find the selection rule for admissible lattice distortions that can be involved in this transition

$$\Gamma_{15}^- \otimes \Gamma_{25}^+ = \Gamma_{15}^- + \Gamma_{25}^- + \Gamma_2^- + \Gamma_{12}^-. \tag{4.1}$$

Only two of the former modes can be realized as NN distortions in the NaCl lattice. All our fits demonstrate the decisive part of Γ_{25}^- in describing the TO[ξ00] anomaly.

The conventional dipole distortion mode Γ_{15}^- mainly influences the longitudinal branches of the vibration spectrum. This contribution, however, softens LO phonons mainly in the vicinity of the Γ point. To describe the total softening of the LO branch one must also include the even Γ_1^+ mode (see figures 2 and 5 in KMII).

It is noteworthy that the non-locality of monopolar Γ_1^+ exciton manifesting itself in the covalent factor $R_{\Gamma_1^+}(q)$ (see equation (2.8)) improves both the theoretical description of the neutron scattering data for dispersion curves and the calculations of elastic moduli. This factor can be represented in the form (KMI, KMII)

$$R_{\Gamma_1^+}(q) = \sum_{R_m}^{NN} (1 - \cos q \cdot R_m) \tag{4.2}$$

which turns into zero in the long-wave limit $q \to 0$. This symmetry rule makes the moduli c_{11} and c_{12} insensitive to the breathing mode influence, contrary to the usual local CDD model (see e.g. Mahler and Engelhardt 1971). Hence, in our hybrid iteration procedure where the elastic moduli are used for defining the microscopic constants (see appendix), the contribution of the covalent factor is particularly important.

All iteration regimes used in our calculations are listed in table 1. Table 2 contains the parameters of the dynamic matrix and the calculated values of the long-wave data. To check our approach we used several fitting procedures (columns A to F in tables 1 and 2).

(i) Models A and B use the hybrid method of the appendix. When including the non-local corrections for Γ_1^+ CDD mode (model B) the RMS was 22% better than in the case of $R_{\Gamma_1^+} \equiv 1$ (model A). The calculated phonon spectrum of model B demonstrates slight deviations from the experimental data for TA[100] and LA[111] branches, although the general consistency is rather satisfactory.

(ii) The free fit of models C and D starts from the value of dipole rigidity K_2 of the sulphur shell, which is taken from the EuS fitting; all other parameters are obtained along the procedures of models A and B, respectively. The assumption of K_2 invariability is justified by the proximity of dipole excitation energies of S ions in both sulphides. As a result the RMS deviation for the 'covalent' model D is 10% better than for the 'conventional' model C. We find therefore that the decrease of RMS deviation due to

Table 1. The models of $SmS_{(B)}$ spectrum fit: 1, Sm ion; 2, S ion; F, fitted phenomenological constants; M, the constants calculated in the hybrid method using the macroscopic data and fitted F constants (see appendix).

		A	B	C	D	E	F
Full	A_{12}	M	M	F	F	F	F
ion–ion	B_{12}	M	M	F	F	F	F
interaction	A_{11}	F	F	F	F	F	F
	B_{11}	F	F	F	F	F	F
	A_{22}	M	M	F	F	F	F
	B_{22}	M	M	F	F	F	F
Shell–shell	T_{12}	F	F	F	F	F	F
interaction	D_{12}	F	F	F	F	F	F
	T_{11}	F	F	F	F	F	F
	D_{11}	F	F	F	F	F	F
	T_{22}	F	F	F	F	F	F
	D_{22}	F	F	F	F	F	F
CDD	K_1	M	M	F	F	F	F
parameters	K_2	M	M	EuS	EuS	F	F
	G_1	F	F	F	F	F	F
	G_{25}	F	F	F	F	F	F
Ion and	Z	F	F	F	F	F	F
shell	Y_1	M	M	F	F	F	F
charges	Y_2	M	M	F	F	F	F
Covalent	$R_{\Gamma\dagger}$						
factor	Φ_1	no	yes	no	yes	no	yes

involving the covalent factor is more essential for the hybrid method (22%) using the macroscopic constants in the fitting procedure. This is because the non-local breathing mode unlike the conventional one does not contribute to elastic moduli. The macroscopic parameters obtained in these two models are close enough to the experimental values. The phonon dispersion curves of model D are plotted in figure 2.

(iii) In models E and F the parameter K_2 was also variable, but both RMS deviations and final K_2 values are practically the same as in the models C and D, respectively, which confirms the assumption of invariability of the S ion dipolar rigidity in both sulphides.

Our preliminary calculations of the $SmS_{(B)}$ phonon spectra based on the second-order perturbation theory (KMI, KMII) predicted that the softening of LO phonon modes is ensured by the mutual action of the local dipolar and non-local monopolar CDD modes. A more accurate solution of dynamic equations confirms this picture and shows the overall 1 THz softening of LO[$\xi\,\xi\,\xi$] mode. The essential role of the covalent contribution is demonstrated by the models B, D and F in comparison with the models A, C and E, respectively. As follows from the general theory (KMI, KMII) the enhancement of non-local Γ_1 excitation is responsible for the softening of LO(L) vibration, in comparison with the EuS spectrum, and the softening of LO(Γ) phonon is the direct consequence of the softening of electronic f–d transitions in RE open shells, although in model B the change in the Sm–S coupling constant also plays an essential part. In all the models the polarizability of Sm ions is practically the same ($\alpha_1 = 3.24$–3.33 Å^3) and exceeds substantially that for Eu ions ($\alpha_1 \simeq 2.47$ Å^3).

Table 2. Microscopic and macroscopic parameters of the models of table 1. Experimental values of elastic moduli (Denier *et al* 1976), high-frequency dielectric constant ε (Güntherodt and Holtzberg 1976) and sulphur polarizability α_2 (Tessman *et al* 1953) correspond to first and second columns of the table (hybrid method). The polarizability α is in Å^3. Here and in subsequent tables the forces and CDD constants are in $e^2 V^{-1}$, the elastic moduli are in 10^{12} dyn cm^{-2} and δ is the RMS deviation for the experimental points included in the fit in THz.

	A	B	C	D	E	F
A_{12}	18.2	16.1	19.9	20.0	20.0	20.1
B_{12}	−2.53	−1.98	−2.76	−2.84	−2.73	−2.86
A_{11}	0.522	0.292	0.803	0.644	0.843	0.766
B_{11}	−0.051	−0.036	−0.310	−0.285	−0.321	−0.328
A_{22}	−1.78	−1.34	−2.24	−2.16	−2.22	−2.15
B_{22}	0.45	0.442	0.675	0.705	0.655	0.732
T_{12}	20.4	20.4	22.5	22.2	22.5	22.2
D_{12}	−3.05	−3.09	−2.97	−2.89	−3.02	−2.78
T_{11}	0.123	−0.465	2.36	1.92	2.32	2.09
D_{11}	−0.381	−0.603	−1.31	−1.27	−1.21	−1.31
T_{22}	−1.86	−2.42	−1.59	−1.88	−1.60	−2.01
D_{22}	0.286	0.022	−0.726	−0.791	−0.691	−0.862
K_1	203	299	219	217	212	218
K_2	140	206	135	135	127	142
G_1	1.05	1.34	0.654	0.876	0.620	1.06
G_{25}	0.335	0.383	0.355	0.200	0.336	0.100
Z	1.83	1.68	1.96	1.97	1.96	1.97
Y_1	4.07	4.74	4.36	4.36	4.36	4.36
Y_2	−4.07	−4.74	−4.43	−4.38	−4.40	−4.46
C_{11}	1.200	1.200	1.262	1.308	1.272	1.330
C_{12}	0.110	0.110	0.179	0.213	0.193	0.232
C_{44}	0.250	0.250	0.290	0.288	0.292	0.292
B	0.470	0.470	0.540	0.578	0.553	0.598
ε	6.000	6.000	7.854	7.632	8.568	7.556
ε_0	10.53	10.531	13.391	13.298	14.344	13.253
α_1	3.24	3.24	3.30	3.33	3.36	3.33
α_2	4.70	4.70	5.54	5.42	5.74	5.39
δ	0.149	0.122	0.096	0.087	0.096	0.086

Thus one can conclude that it is the softening of the excitonic spectrum involving the transitions in Sm open shells that is responsible for the renormalization of the phonon spectrum in a narrow-gap semiconductor $SmS_{(B)}$ in comparison with that in a wide-gap semiconductor EuS. Two of these excitons (Γ_{15}^- and Γ_{25}^-) can be treated as local Frenkel states, but the monopole exciton is essentially non-local.

5. Cation-substituted $Sm_{1-x}R_xS$ and high-pressure phase $SmS_{(G)}$

Exciton softening is expected to be particularly prominent in the mixed-valence semiconductors. Moreover, the soft breathing mode according to the theory of excitonic

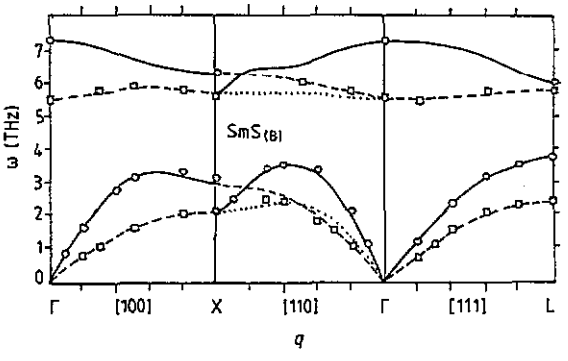

Figure 2. Calculated phonon spectrum of $SmS_{(B)}$ fitted within model D of tables 1 and 2 including the covalent factor. The value of K_2 is the same as for the EuS spectrum. The experimental points are denoted by: (○) LO, LA; (□) TA_1, TO_1. Other symbols as in figure 1.

instability plays the key part in formation of the ground state of the MV semiconductor (Stevens 1976, Kikoin 1984). Therefore it is natural to conjecture an essential contribution of electron(exciton)–phonon interaction (EPI) to the phonon renormalization in those systems. The most famous and thoroughly investigated MV compound is cation-substituted SmS. It is the chemically collapsed solid solution $Sm_{0.75}Y_{0.25}S$, where distinct anomalies in longitudinal phonon branches and extra dispersionless mode were found for the first time in the neutron scattering experiment (Mook *et al* 1978). Later on, similar anomalies in LA branch were discovered also in MV 'gold SmS' ($SmS_{(G)}$) under hydrostatic pressure (Mook *et al* 1982) and in antiferromagnetic MV semiconductor TmSe (Mook and Holtzberg 1981).

Although the first theoretical explanation of phonon anomalies (Entel *et al* 1979, Bilz *et al* 1979a) did not distinguish between the MV states induced by external pressure and chemical substitution, more detailed analysis reveals quite different behaviour of LA and LO branches in the two cases. Our approach enlightens these distinctions and admits the modifications taking into account the specific features of pure MV semiconductor and heavily doped solid solution.

When analysing the EPI in narrow-gap $SmS_{(B)}$ we have discovered the essential contribution of covalent factor $R_\Gamma(q)$ in phonon renormalization. This contribution is enhanced substantially in MV SmS (see KMI, KMII), and it has different q dependence in perfect and doped systems. The latter difference is very important because it can be revealed directly in a neutron scattering experiment. Indeed, in a perfect system that possesses the symmetry of the point crystal group this q dependence is determined by selection rules (cf equations (2.6) and (4.2)), which forbid the on-site electronic transitions under the influence of fully symmetric lattice distortion (the envelope function $F(l)$ has a node on a central site). However, the lattice defects or impurities weaken this rigid restriction owing to lowering of the point symmetry in a cell containing such a defect. The factor $R_{\Gamma_1^+}(q)$ was calculated in KMI for the case of two-band f–d semiconductor, and the corresponding equation (4.3) of that paper can be generalized for the case of an imperfect lattice. This generalization results in a second-order covalent contribution to the phonon softening:

$$\Phi_1^{(\Gamma_1)} = E_{ex}^{-1}(q)[\![F_0 + F_1[Z - S(q)]\{F_1[A^2 + |VG_0|^2 S(q)]\,\tfrac{1}{2}\sin(2\theta)$$

$$+ A|V|g_0\cos(2\theta)\}]\!]^2. \tag{5.1}$$

Here $F_{0,1}$ are the envelope functions on the central and NN sites, respectively, $S(q)$ is a structure factor

$$S(q) = \sum_{l}^{NN} \exp(iq \cdot R_l) \tag{5.2}$$

g_0 is a Green function

$$g_0 = N^{-1} \sum_{k} (E_{ck} - E_{vk})^{-1} \tag{5.3}$$

V is the hybridization matrix element defining the dispersion $E_{c,v}$ of the conduction and valence bands of a two-band semiconductor, Z is the coordination number, A is the normalization factor for the band wavefunction defined in a NN tight-binding approximation by the equation $A^2 + Z|Vg_0|^2 = 1$, and θ is the measure of fractional valence. The additional contribution F_0 in the double brackets of (5.1) imitates the contribution of on-site transitions allowed in the defect lattice.

The q dependence in Φ_1 is determined mainly by the factor $[Z - S(q)]$ at any realistic values of A, V and θ (see KMI); hence the degree of imperfection can be characterized by the parameter

$$\kappa^{-1} = F_1 F_0^{-1}[\tfrac{1}{2}\sin(2\theta)F_1 + |V|G_0\cos(2\theta)]. \tag{5.4}$$

The phonon spectra for MV phase of SmS were calculated within the same scheme as those for black $SmS_{(B)}$, but with additional fitting parameter κ. Besides, it was necessary to introduce a coupling constant $G_1(11)$ describing the contribution of NN Sm ions to the breathing CDD in addition to Sm–S coupling constant $G_1(12)$ and non-central RI NNN forces α, β, γ instead of the central-type interactions in semiconducting $SmS_{(B)}$. Both these interactions are induced by essentially delocalized open shells of Sm ions in the MV state.

However, this approach has turned out to be insufficient for describing the optical branches accurately (see below); hence we have excluded from our fitting procedure the dipole CDD mode, which influences mainly the optical phonons, and have focused our attention on revealing the role of breathing CDD mode Γ_1^+ in LA anomalies.

When extracting the model parameters from the experimental data we ran into the problem of the lack of experimental information on the phonon spectra of the high-pressure phase of $SmS_{(G)}$. Only direct neutron measurements for LA branch (Mook *et al* 1982) and optically determined frequencies in LO(Γ) and LO(L) points (Travaglini and Wachter 1985, Güntherodt *et al* 1978) are available. Some additional information can be extracted from the LA(L) and $LA_{100}(X)$ frequencies, which are known for both black and gold phases. Experimentally detected vibration hardening of these frequencies in the gold phase could be ascribed to the change of RI parameters due to lattice collapse because the CDD(Γ_1^+) contribution is symmetry-forbidden just for these points. Hence we use the scaling coefficient

$$\omega^2_{L,LA}(G)/\omega^2_{L,LA}(B) \simeq \omega^2_{X,LA}(G)/\omega^2_{X,LA}(B) = 1.37$$

for obtaining the shift of TA branches of $SmS_{(G)}$ from the known frequencies for $SmS_{(B)}$ (TA branches are not disturbed by the breathing CDD mode). Figures 3 and 4 show the results of theoretical fitting together with the experimental data for the phonon spectra of $SmS_{(G)}$ under pressure and $Sm_{0.75}Y_{0.25}S$.

Thus, our calculations show the relative contribution of both mixed-valence and imperfection effects. Our previous analyses (KMI, KMII) have demonstrated that without

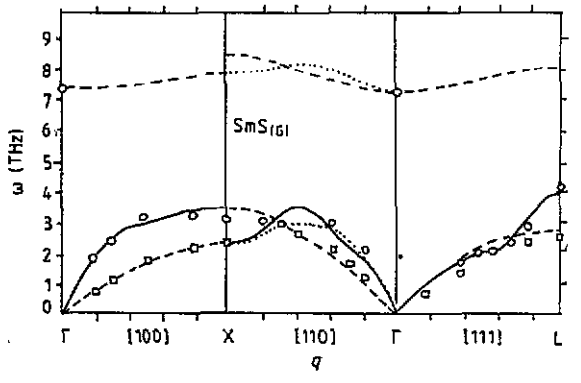

Figure 3. $SmS_{(G)}$ phonon spectrum calculated in model B of table 4. Symbols as in figure 2.

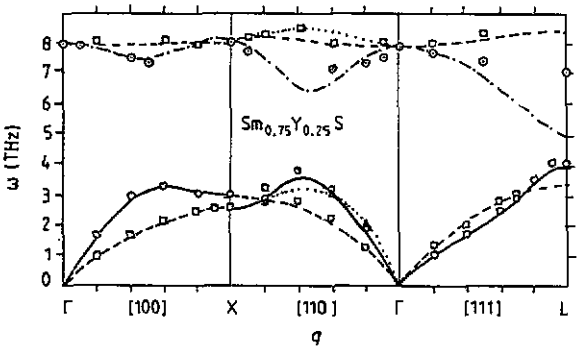

Figure 4. $Sm_{0.75}Y_{0.25}S$ phonon spectrum calculated in model B of table 3: (⊙) experimental LO points that are excluded from the fitting procedure; (△) experimental TA_2 points. Calculated LO branch is shown by the chain curve. Other symbols as in figure 2.

taking into account the covalent factor the anomalous dispersion of the LA branch cannot be described correctly; the standard CDD(Γ_1) model gives maximum phonon renormalization in the middle of the ΓL direction in the Brillouin zone, whereas the covalent contribution shifts this maximum towards the L point in accordance with the experiment. Here we see that the imperfection 'smoothes' the q dependence of $\Phi_1(q)$. This effect can be described by the simplified equation (5.1) using parameter κ from (5.4):

$$\Phi_1^{(\Gamma_1^+)}(q) \sim \{1 + \kappa^{-1}[Z - S(q)]\}^2. \tag{5.5}$$

Figure 5 illustrates this smoothing quantitatively.

As a result in more dirty $Sm_{0.75}Y_{0.25}S$ the covalency effect is manifested less sharply than in the high-pressure $SmS_{(G)}$ (see figures 6(*a*) and (*b*)). In very dirty crystals ($\kappa \to \infty$) the symmetric q dependence prescribed by the point CDD model (Matsuura *et al* 1980) for the LA phonon renormalization $\delta\omega_{LA}(q)$ should be restored. Quantitatively, this picture is seen from tables 3 and 4. The RMS deviation is essentially lower for model B, which involves the covalent factor (5.5), than for model A, based on conventional point CDD theory, whereas the value of κ in the best fits for $Sm_{0.75}Y_{0.25}S$ is a factor 14 higher than that for $SmS_{(G)}$.

It should be emphasized that the imperfection also influences the contribution of CDD modes to the elastic moduli. We have seen in the previous section that the symmetry

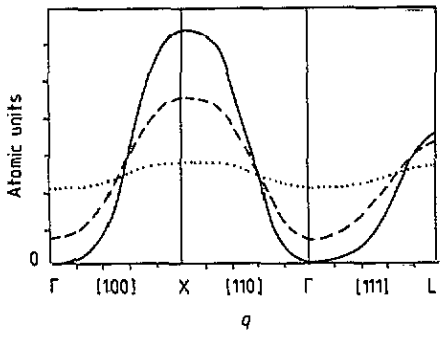

Figure 5. Normalized covalent factor for the NN localization of the excited electron LCAO (linear combination of atomic orbitals) in the NaCl lattice for the various values of the imperfection parameter κ: $\kappa = 0$ (——); $\kappa = 10$ (– – –); $\kappa = 100$ (· · · · ·). $R \equiv 1$ for $\kappa = \infty$.

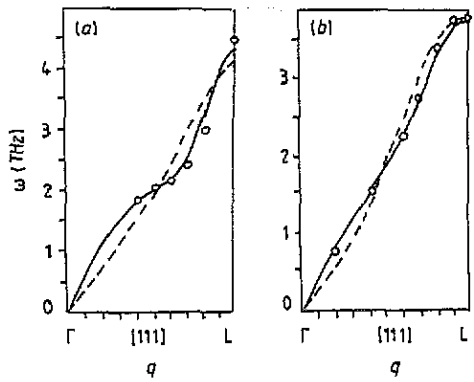

Figure 6. (*a*) LA[$\xi\,\xi\,\xi$] anomaly in $SmS_{(G)}$: (——) model B with the non-local correction; (– – –) local model A (table 4). (*b*) LA[$\xi\,\xi\,\xi$] anomaly in $Sm_{0.75}Y_{0.25}S$: (——) model B with the non-local correction; (– – –) local model A (table 3).

Table 3. Microscopic parameters and elastic properties of $Sm_{0.75}Y_{0.25}S$ fitting models (see notation in table 2). The experimental elastic moduli alter for the various samples and temperatures. The ranges of experimental values are taken from Denier *et al* (1976), Mook *et al* (1978) and Mook and Holtzberg (1981).

	A	B	C	D	
A_{12}	8.40	8.29	8.23	8.50	
B_{12}	1.18	1.22	1.23	1.05	
α_{11}	0.031	0.043	0.041	0.172	
β_{11}	0.98	0.87	0.69	0.76	
γ_{11}	0.153	0.170	0.118	0.086	
α_{22}	0.363	0.365	0.316	0.309	
β_{22}	−1.25	−1.38	−1.06	−0.89	
γ_{22}	0.44	−0.02	0.087	0.132	
$G_1(12)$	1.44	0.757	0.00	0.00	
$G_1(11)$	0.395	0.766	0.563	1.30	
κ	–	9.41	–	7.75	
LO	not fitted				
δ	0.107	0.094	0.169	0.157	
	Calculated				Experimental
C_{11}	1.185	1.437	1.135	1.457	0.98 to 1.35
C_{12}	−0.849	−0.67	−0.897	−0.574	−0.35 to −0.50
C_{44}	0.31	0.31	0.31	0.31	0.29 to 0.31
B	−0.171	0.03	−0.220	0.103	0.05 to 0.16

Table 4. Microscopic parameters and elastic properties of $SmS_{(G)}$ fitting models (see notation in table 2). The experimental value of B is taken from Keller *et al* (1979).

	A	B	
A_{12}	8.31	8.07	
B_{12}	0.32	0.69	
α_{11}	0.72	0.79	
β_{11}	1.48	1.49	
γ_{11}	−0.23	−0.36	
α_{22}	0.65	0.62	
β_{22}	−1.12	−1.18	
γ_{22}	−0.13	−0.04	
$G_1(12)$	2.10	1.44	
$G_1(11)$	0.495	2.32	
κ	–	0.66	
δ	0.230	0.187	
	Calculated		Experimental
C_{11}	1.379	1.925	–
C_{12}	−0.689	−0.193	–
C_{44}	0.236	0.297	–
B	0.0007	0.513	0.52

rules cancel out the influence of the on-site electronic transitions on the long-wave part of acoustic branches. The violation of the point crystal symmetry by impurities and intrinsic defects removes this restriction. As a result we obtain a noticeable contribution to the moduli C_{11} and C_{12}, which depends on the degree of imperfection. Experimentally, the bulk modulus B in the high-pressure $SmS_{(G)}$ is larger than in the cation-substituted $Sm_{1-x}Y_xS$ (see tables 3 and 4). We suppose that the disorder-induced contribution to the long-wave acoustic phonons is responsible for this difference. Indeed, the fitting procedure for $SmS_{(G)}$ with small value of κ (model B of table 4) gives excellent agreement with the experimental value of B, whereas the point CDD model A gives a lattice close to instability. The same procedure results in satisfactory theoretical description of the elastic tensor for highly imperfect $Sm_{0.75}Y_{0.25}S$ (model B of table 3 with covalent contribution). The point CDD model A gives a statically unstable lattice ($B < 0$).

It is instructive that in the most successful models A and B we were forced to exclude the experimental LO points from the fitting procedure. In these models the LO branch turns out to be softened essentially near the L point almost right to closing the gap between optic and acoustic parts of the phonon spectrum, in dramatic disagreement with experiment (see figure 4). Our attempts to include the LO phonons in the fitting procedure with and without non-local corrections (models C and D for $Sm_{0.75}Y_{0.25}S$) resulted in an unreasonable picture for the breathing CDD contribution; the coupling constant for CDD-induced NN Sm–S interaction $G_1(12)$ tends to zero, and one should ascribe all anomalies to NNN interaction, which seems to be an unphysical result.

We think that the failure of our non-local CDD model in the description of the LO branch is connected with the essentially non-adiabatic regime of interaction between

Table 5. Microscopic parameters and elastic properties of TmSe fitting models (see notation in table 2). The values of elastic moduli are determined from the long-wave part of the phonon spectrum (Mook and Holtzberg 1981).

A_{12}	8.89
B_{12}	0.25
α_{11}	0.55
β_{11}	0.81
γ_{11}	−0.20
α_{22}	0.42
β_{22}	−0.25
γ_{22}	0.15
$G_1(12)$	1.96
$G_1(11)$	0.80
κ	24.5
δ	0.142

	Calculated	Experimental
C_{11}	1.476	1.85
C_{12}	−0.445	−0.65
C_{44}	0.206	0.26
B	0.195	0.18

the optical phonons and the breathing electronic mode. A conventional adiabatic picture should fail for the case of extremely soft electronic (excitonic) transitions involved in CDD modes. Apparently, the resonance mode in the gap between the optic and acoustic branches (Mook *et al* 1978, Stüsser *et al* 1982) is the direct manifestation of this non-adiabaticity. In a forthcoming paper, the non-adiabatic EPI will be included in the theoretical description. Preliminary calculations show that insertion of the resonance interaction removes the discrepancies between the theory and experiment for the LO branch.

6. Thulium selenide

The phonon spectrum of TmSe demonstrates the same anomalies as all other MV rare-earth compounds with NaCl structure, i.e. the 'dip' in the LA[1 1 1] branch and negative C_{12} modulus (Mook and Holtzberg 1981). As to the gap dispersionless mode, the experimental situation is still uncertain (Stüsser *et al* 1982). The specimen used in the neutron scattering experiment was even more imperfect than the $Sm_{0.75}Y_{0.25}S$ sample, and the value of the imperfection parameter $\kappa = 24.5$ in our best fit (table 5, figure 7) reflects this situation. Taking into account the covalent factor gives no essential improvement in comparison with the conventional point CDD(Γ_1) model (cf section 5). One point on the LA[1 0 0] branch 'slips' out of the theoretical curve, but it is unclear whether this discrepancy results from the theoretical shortcomings or from the experimental uncertainty.

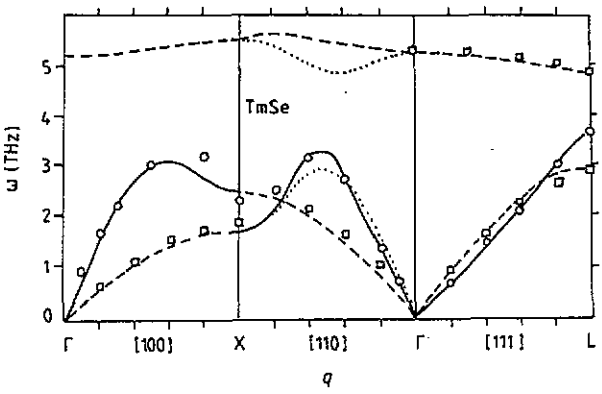

Figure 7. Calculated phonon spectrum of TmSe. Symbols as in figure 2.

7. Summary

All the above results together with the successful description of the phonon spectra of SmB_6 within the same theoretical approach (Alexeev *et al* 1989) corroborate the reliability of the excitonic mechanism of the mixed-valence fluctuations, which are responsible for both the phase transition to MV phase and the anomalous phonon renormalization in RE semiconductors with unstable valence. Moreover, our understanding of the microscopic nature of this phenomenon permits us to analyse critically the previous approaches to EPI in these systems.

Early rough phenomenological theory involving local Γ_1^+ and Γ_{15}^- CDD modes (Bilz *et al* 1979) seizes the main anomalies of the phonon spectra but the model seems to be oversimplified to extract all essential physical information from the theoretical description. For example, the coupling constants for Γ_1^+ and Γ_{15}^- modes are taken to be equal because both dipole and monopole fluctuation modes were assumed to be highly localized. As a result the role of the dipole mode was exaggerated, and in the LA(L) point where the Γ_1^+ mode gives no contribution, the theory gave 15% discrepancy with experiment. Our microscopic approach predicts essentially more delocalized breathing mode, and easily removes this discrepancy. The model of Bilz *et al* draws also on the Γ_{12}^+ sulphur polarizability to describe the LA(L)–TA(L) splitting. However, this mode was not registered in the Raman spectra of $Sm_{0.75}Y_{0.25}S$ (Güntherodt *et al* 1981b). Apparently, this splitting is connected with the screened Coulomb forces, because inclusion of this contribution to the dynamic matrix gives overall agreement between the experiment and theory (cf the Born–von Karman fitting by Mook and Nicklow (1979)), with the exception of the anomalies in longitudinal branches.

The importance of Coulomb interaction is confirmed by increased LA(L)–TA(L) splitting in gold SmS in comparison with cation-substituted $Sm_{0.75}Y_{0.25}S$ because the screening in the latter is more effective due to the donor properties of component Y. Besides, one can mention the increase of LA(X)–TA(X) and $LA,TA_2(M)$–$TA_1(M)$ splitting in the MV semiconductor SmB_6 (Alexeev *et al* 1989) in comparison with that in metallic LaB_6 (Smith *et al* 1985). Another contribution to LA-TA splitting in the ΓL direction should be provided by the f–d hybridization matrix element dependence on the bond bending between NN Sm ions (Grewe and Entel 1979).

Thorough calculations of vibrational spectrum including phonon damping were published by Wakabayashi (1980). He restricted himself to a conventional adiabatic scheme and described the damping by introducing a phenomenological relaxation time. However, he had to include additional breathing CDD of sulphur shells to obtain a satisfactory description of anomalies in the longitudinal branches. Apparently, this artificial mode imitates the real breathing CDD distortions of Sm shells induced by the motion of NNN of the central Sm ion (see $G_1(11)$ in tables 3 and 4). Nevertheless, we recalculated the phonon spectrum of SmS within the Wakabayashi model, and found that the RMS minimum with his fitting parameters really is a local extremum, which allows further reduction by continuing the iteration process.†

Previous attempts at a microscopic description of EPI were undertaken by Bennemann and Avignon (1979) and Matsuura *et al* (1980). However, both models used the one-centre approximation for electronic transitions and neglected the q dependence of the denominator in the electronic susceptibility. Hence, eventually, these attempts have returned back to the phenomenological description of the local CDD theory.

The only attempt at a non-local description was developed by Entel *et al* (1979), who used explicitly the parity ban on the intrasite f–d transitions. But when constructing the non-local intersite hybridization matrix elements, Entel *et al* (1978) neglected the real transformation properties of the d orbital (cf KMI), and obtained an incorrect q dependence of the matrix elements. However, further calculations of phonon renormalization did not exploit this dependence because the main effect was ascribed to the influence of Y impurities, which breaks the inversion symmetry in the crystal elementary cell and allows local electronic transitions in the RE shells. Finally the model again returns to the local description of conventional CDD theory.

The Green function theory of Kuroda and Bennemann (1981) goes beyond the adiabatic approximation in describing the EPI induced by the local f–d transitions. This treatment seems to be the most promising for describing the interaction between the soft excitations in the electron subsystem and the optical phonons, provided the non-local transitions are taken into account. This route is preferable for describing the resonance mode in comparison with the effective local vibration model ascribing finite mass to the electron mode (Pastor *et al* 1987).

In conclusion, we tried to trace the evolution of local electronic contribution to the phonon spectra renormalization in a sequence of RE semiconductors from EuS with stable valence to $SmS_{(G)}$ with mixed valence, and revealed the decisive part of characteristic excitonic-type modes describing the monopole and dipole f shell distortions. The prominent breathing mode in these systems turns out to be essentially non-local, and just in the phonon spectra this non-locality manifests itself most graphically. Hence, one can verify the microscopic models of valence fluctuations by studying the anomalies in the phonon dispersion curves.

Appendix

One often meet the situation of incomplete experimental data on phonon spectra. The extreme case is the absence of neutron scattering measurements of the phonon dispersion

† The phonon spectrum presented in figure 2 of Wakabayashi (1980) cannot correspond to his best-fit parameters, because at zero Sm–Sm interaction parameters of RI model the LA(L) and TA(L) frequencies have to be degenerate.

curves when only elastic moduli and maybe infrared optical data are available. In this case the model parameters defining the dynamic matrix should be determined from the macroscopic data in a unique way. When one can also use information on some phonon branches a 'hybrid' procedure can be proposed that combines the free fitting to the experimental curves by varying the model parameters with derivation of some parameters from the macroscopic data and above variable parameters. This method is competitive even in the case of full experimental information on the dispersion curves because it reduces the effective 'dimension' of the parameter space in the fitting procedure and optimizes the consistency between the macroscopic description of the lattice and the microscopic calculation of the phonon branches.

When describing the phonon spectra of $SmS_{(B)}$ along the Zeyher and Kress (1979) procedure in section 4 we determined uniquely the microscopic parameters from seven macroscopic quantities, i.e. elastic moduli C_{11}, C_{12}, C_{44}, frequencies $\omega_{LO}(\Gamma)$, $\omega_{TO}(\Gamma)$, dielectric constant ε_∞ and sulphur ion polarizability α_2. Eight parameters defined in this way are denoted by symbol 'M' in table 1 (two of them are connected, $Y_1 = -Y_2$, hence this procedure is unique). This procedure gives only qualitative consistency with experiment, and therefore it was modified by using the above hybrid approach where all parameters except those denoted by 'M' in columns 1 and 2 of table 1 were fitted to the phonon curves. These parameters are denoted by the symbol 'F'. M parameters were rederived at each step of the fitting procedure from the macroscopic data and variable F parameters. Our procedure allows us both to sustain the consistency of the long-wave part of the phonon spectrum with the macroscopic data and to avoid the unphysical local minima in a multidimensional parameter space during the iteration routine.

In fact, the macroscopic parameters are often measured with large error and disagree with the constants extrapolated from the phonon spectra (see e.g. discussion of the long-wave phonons for alkali halides in Bilz *et al* (1974)). Hence, the RMS minimum found by means of the hybrid method can be used as the starting point for the free fitting procedure. Thus the shortest path to the global minimum can be found.

Here we try the hybrid fitting method for the simple rock-salt lattice. It should be emphasized, however, that this method can be particularly useful for low-symmetry lattices where the search for the global minimum is a much more difficult task due to high dimensionality of the parameter space. The hybrid fitting procedure admits partial compensation of the growing number of parameters because additional independent components of the elasticity tensor predetermine the values of some of these parameters.

References

Alexeev P A, Ivanov A S, Dorner B, Schober H, Kikoin K A, Mishchenko A S, Konovalova E S, Paderno Yu B, Lazukov V N, Rumyantsev A Yu and Sadikov I P 1989 *Europhys. Lett.* **10** 457

Allen B 1977 *Phys. Rev.* B **16** 5139

Bennemann K H and Avignon M 1979 *Solid State Commun.* **31** 645

Bilz H, Buchanan M, Fischer K, Haberkorn R and Schröder U 1975 *Solid State Commun.* **16** 1023

Bilz H, Gliss B and Hanke W 1974 *Dynamical Properties of Solids* ed A A Maradudin and G K Horton (Amsterdam: North-Holland) vol 1, p 343

Bilz H, Güntherodt G, Kleppmann W and Kress W 1979 *Phys. Rev. Lett.* **43** 1998

Bilz H and Kress W 1979 *Phonon Dispersion Relations in Insulators* (Berlin: Springer)

Birgenau R L and Shapiro S M 1977 *Valence Instabilities and Related Narrow Band Phenomena* ed R D Parks (New York: Plenum) p 49

Denier P D, Weber W and Longinotti L D 1976 *Phys. Rev.* B **14** 3635

Entel P, Grewe N, Sietz M and Kowalski K 1979 *Phys. Rev. Lett.* **43** 2002
Entel P, Leder H J and Greve N 1978 *Z. Phys.* B **30** 277
Grewe N and Entel P 1979 *Solid State Commun.* **31** 655
Güntherodt G and Holtzberg F 1976 *Solid State Commun.* **18** 181
Güntherodt G, Jayaraman A, Bilz H and Kress W 1981a *Valence Fluctuations in Solids* ed L M Falicov, W Hanke and M B Maple (Amsterdam: North-Holland) p 121
Güntherodt G, Jayaraman A, Kress W and Bilz H 1981b *Phys. Lett.* **82A** 26
Güntherodt G, Merlin R, Frey A and Cardona M 1978 *Solid State Commun.* **27** 551
Güntherodt G, Merlin R and Grunberg P 1979 *Phys. Rev.* B **20** 2834
Hillebrands B and Güntherodt G 1984 *Solid State Commun.* **47** 681
Ichinose S and Kuroda Y 1982 *Phys. Rev.* B **25** 2550
Ichinose S and Tamura I 1983 *Phys. Status Solidi* b **120** 703
Keller R, Güntherodt G, Holzapfel W B, Dietrich H and Holtzberg F 1979 *Solid State Commun.* **29** 753
Kikoin K A 1984 *J. Phys. C: Solid State Phys.* **17** 6671
Kikoin K A and Mishchenko A S 1988 *Sov. Phys.–JETP* **67** 2309
—— 1990 *J. Phys.: Condens. Matter* **2** 6491
Kuroda Y and Bennemann K H 1981 *Phys. Rev.* B **23** 4114
Lopez-Aguilar F and Costa-Quintana J 1986 *J. Phys. C: Solid State Phys.* **19** 2485
Mahler G and Engelhardt P 1971 *Phys. Status Solidi* b **45** 543
Matsuura T, Kittler R and Bennemann K H 1980 *Phys. Rev.* B **21** 3467
Mook H A and Holtzberg F 1981 *Valence Fluctuations in Solids* ed J M Falicov, W Hanke and M B Maple (Amsterdam: North-Holland) p 113
Mook H A, McWhan D B and Holtzberg F 1982 *Phys. Rev.* B **25** 4321
Mook H A and Nicklow R M 1979 *Phys. Rev.* B **20** 1656
Mook H A, Nicklow R M, Penney T, Holtzberg F and Shafer M W 1978 *Phys. Rev.* B **18** 2925
Pastor G, Caro A and Alascio B 1987 *Phys. Rev.* B **36** 1673
Smith H G, Dolling G, Kunii S, Kasaya M, Liu B, Takegahara K, Kasuya T and Goto T 1985 *Solid State Commun.* **53** 15
Stevens K W H 1976 *J. Phys. C: Solid State Phys.* **9** 1417
Stüsser N, Güntherodt G, Jayaraman A, Fischer K and Holtzberg F 1982 *Valence Instabilities* ed P Wachter and H Boppart (Amsterdam: North-Holland) p 69
Tessman J R, Kahn A K and Shockley W 1953 *Phys. Rev.* **92** 890
Travaglini G and Wachter P 1985 *J. Magn. Magn. Mater.* **47–48** 423
Wakabayashi N 1980 *Phys. Rev.* B **22** 5833
Woods A D B, Cochran W and Brockhouse B N 1960 *Phys. Rev.* **119** 980
Zeyher R and Kress W 1979 *Phys. Rev.* B **20** 2850